Monthly Notices
of the
ROYAL ASTRONOMICAL SOCIETY

MNRAS **484,** L69–L74 (2019) doi:10.1093/mnrasl/sly198

Evidence of a large-scale positive rotation–metallicity correlation in the Galactic thick disc

Paola Re Fiorentin,* Mario G. Lattanzi and Alessandro Spagna

INAF - Osservatorio Astrofisico di Torino, Strada Osservatorio 20, I-10025 Pino Torinese, TO, Italy

Accepted 2018 October 17. Received 2018 October 17; in original form 2018 August 6

ABSTRACT

This study is based on high quality astrometric and spectroscopic data from the most recent releases by *Gaia* and APOGEE. We select 58 882 thin and thick disc red giants in the Galactocentric (cylindrical) distance range $5 < R < 13$ kpc and within $|z| < 3$ kpc, for which full chemo-kinematical information is available. Radial chemical gradients, ∂[M/H]/∂R, and rotational velocity–metallicity correlations, $\partial V_\phi/\partial$[M/H], are re-derived firmly uncovering that the thick disc velocity–metallicity correlation maintains its positiveness over the 8 kpc range explored. This observational result is important as it sets experimental constraints on recent theoretical studies on the formation and evolution of the Milky Way disc and on cosmological models of Galaxy formation.

Key words: Galaxy: abundances – Galaxy: disc – Galaxy: formation – Galaxy: kinematics and dynamics.

1 INTRODUCTION

Although the existence of a thick disc in the Milky Way (MW) was revealed 35 yr ago (Gilmore & Reid 1983) and its spatial, kinematic, and chemical properties are today better defined, its origin is still a matter of debate.

Proposed scenarios include the heating of a pre-existing thin disc through a minor merger (Villalobos & Helmi 2008), accretion of dwarf galaxies stars from disrupted satellites (Abadi et al. 2003), or stars formed *in situ* from gas-rich mergers at high redshift (Brook et al. 2005; Haywood et al. 2015). On the other hand, simulations suggest that thick discs could be produced through secular radial migration of stars induced by spiral arms (Roskar et al. 2008; Schoenrich & Binney 2009; Curir et al. 2012) and flaring combined with inside-out disc formation (Minchev et al. 2017). Such models predict characteristic trends on the kinematics and chemical abundances that can be used to discriminate the one, or the ones, favoured by the MW.

Indeed, detailed information can be obtained from massive astrometric and spectroscopic surveys. Quite recently, the European Space Agency's *Gaia* mission has made its second data release, or *Gaia* DR2 (Gaia Collaboration 2018); it provides unprecedented accurate measurements of parallax and proper motion for more than 1.3 billion stars across the whole sky (Lindegren et al. 2018). On the other hand, as part of SDSS-IV, the Apache Point Observatory Galactic Evolution Experiment fourteenth data release, APOGEE DR14, has delivered high-resolution ($R \sim 22\,500$) high signal-to-noise near-infrared spectra, enabling the determination of precise radial velocities as well as stellar parameters and abundances for more than 20 chemical elements (Majewski et al. 2017; Abolfathi et al. 2018). Finally, we recall that the APOGEE Survey targeted mostly red giant stars (Zasowski et al. 2013).

In this Letter, we take advantage of these new superb measurements to improve on the recent work of Kordopatis et al. (2017) based on APOGEE DR12. Section 2 describes our selection of disc stars, Section 3 presents the findings that resulted from our analysis, while Section 4 addresses the theoretical implications of our results.

2 DATA AND SAMPLE SELECTION

This study starts with a new kinematic catalogue, assembled after cross-matching *Gaia* DR2 and APOGEE DR14. The resulting sample contains DR2 positions, parallaxes and proper motions (Lindegren et al. 2018) plus radial velocities and chemical abundances derived with the APOGEE Stellar Spectra Parameter Pipeline (e.g., Holtzman et al. 2015; Garcia et al. 2016). The data set allows us to derive a complete, six-dimensional phase-space information for a sufficiently *pure* sample of tracers of the disc (thin and thick) populations.

We first select only objects having astrometric solutions that are either not affected by excess of noise, $\varepsilon = 0$, or with a significance level on ε less than two, to discard astrometric binaries and other anomalous cases (see Lindegren et al. 2018, for details). Then, we retain only those stars with relative parallax error $\sigma_\varpi/\varpi < 0.2$ that allows to compute distances as $d = 1/\varpi$ with quasi-Gaussian errors. As for the selection on the APOGEE DR14 data, we reject stars with flags warning of poor stellar parameter estimates, and those with signal-to-noise ratios lower than 70. Also, in order to

* E-mail: paola.refiorentin@inaf.it

© 2019 The Author(s)
Published by Oxford University Press on behalf of the Royal Astronomical Society

Downloaded from https://academic.oup.com/mnrasl/article/484/1/L69/5142291 by guest on 30 November 2020

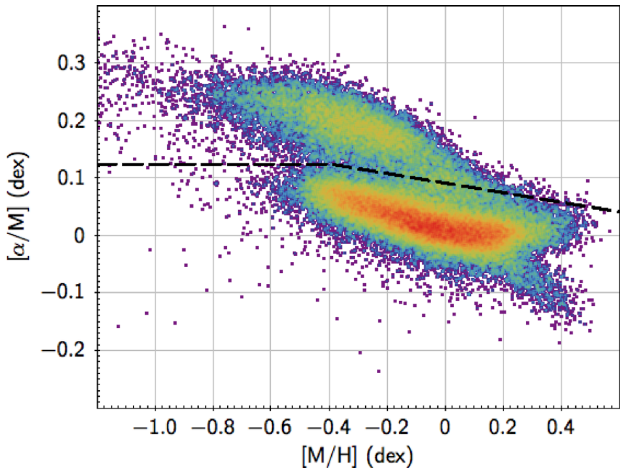

Figure 1. Chemical distribution, [α/M] versus [M/H], for the 67 358 *Gaia* DR2-APOGEE DR14 stars with [M/H] > -1.2 dex and $|z| < 3$ kpc. The dashed line represents the adopted separation between thin disc (below) and thick disc (above). The typical errors are below 0.03 dex per [α/M] and less than 0.07 dex per [M/H].

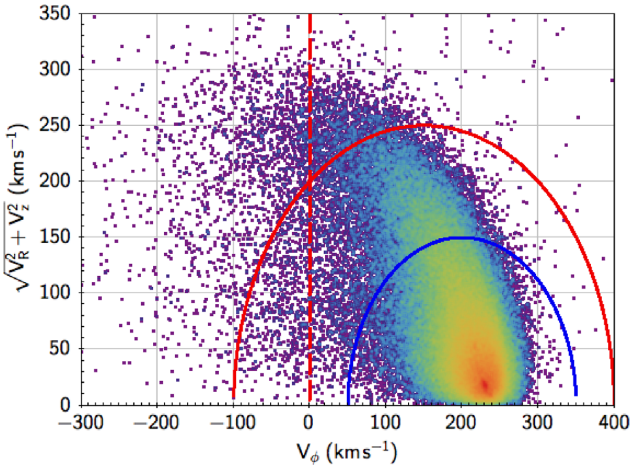

Figure 2. Toomre diagram of the disc sample in Fig. 1. The circles define the Toomre inequalities (see end of Section 2) we used to minimize contamination from halo stars for the thin (blue) and the thick (red) discs. The vertical line, $V_\phi = 0$, is further used to reject halo (retrograde) stars that can contaminate the thick disc sample.

work with reliable α-element abundances, we only consider stars with $\chi^2 < 10$ and $4000 < T_{\rm eff} < 5000$ K according to Anders et al. (2014). Therefore, our initial sample comprises a total of 69 400 red giants down to $G = 17.73$ mag with only 26 stars fainter than 16.5 mag. Median uncertainties are: 0.03 mas in parallax, 50 µas in annual proper motion, and $\sim$100 m s^{-1} for the APOGEE provided line-of-sight velocities.

Three-dimensional velocities in Galactocentric cylindrical coordinates, (V_R, V_ϕ, V_z), are derived by assuming that the Sun is 8.5 kpc away from the MW centre, the LSR rotates at 232 km s^{-1} around the Galactic centre (McMillan 2017), and the LSR peculiar velocity of the Sun is $(U, V, W)_\odot = (11.1, 12.24, 7.25)$ km s^{-1} (Schoenrich, Binney & Dehnen 2010). Median uncertainties of the derived Galactocentric velocities are $(\sigma_{V_R}, \sigma_{V_\phi}, \sigma_{V_z}) = (0.53, 0.64, 0.54)$ km s^{-1}.

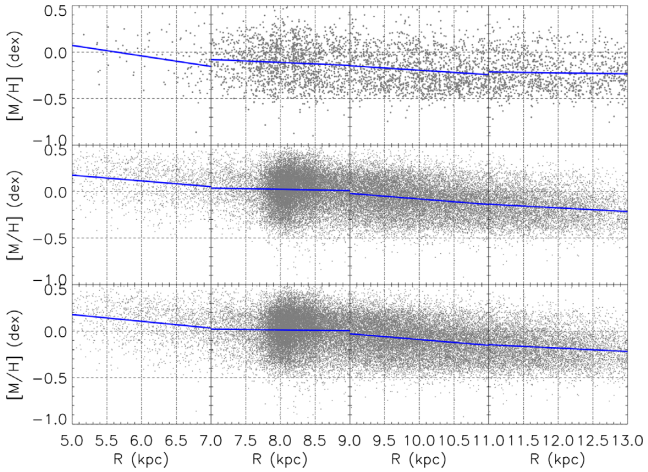

Figure 3. Radial metallicity distribution of thin disc stars in the Galactocentric (cylindrical) distance in the range $5 < R < 13$ kpc and within $|z| < 3$ kpc. From left to right, the full radial range is shown in four 2 kpc wide rings at $R = 6$, 8, 10, 12 kpc. The sample is also divided in three height intervals: $|z| < 3$ kpc (bottom panels), $|z| < 1$ kpc (middle panels), and $1 \leq |z| < 3$ kpc (top panels). The solid lines represent the linear fits to the data.

Disc stars are chemically selected utilizing the constraint [M/H] > -1.2 dex[1] and $|z| < 3$ kpc, resulting in a sample of 67 358 objects. Fig. 1 shows the chemical plane, [α/M] versus [M/H], for this sample; the thin disc (low-α) and thick disc (high-α) subsamples are reasonably well separated (below and above the dashed line, respectively) by the relation:

$$[\alpha/\mathrm{M}] = \begin{cases} +0.125 & \text{if } [\mathrm{M/H}] < -0.4 \\ -0.083([\mathrm{M/H}] - 0.5) + 0.05 & \text{if } [\mathrm{M/H}] \geq -0.4\,. \end{cases} \quad (1)$$

In order to minimize kinematic contamination from the halo, we retain only stars with $V_\phi > 0$ and apply the Toomre selections (see Fig. 2):

$$(V_\phi - 200)^2 + V_R^2 + V_z^2 < 150^2 \text{ km}^2 \text{ s}^{-2} \quad (2)$$

$$(V_\phi - 150)^2 + V_R^2 + V_z^2 < 250^2 \text{ km}^2 \text{ s}^{-2} \quad (3)$$

for thin disc (equation 2) and thick disc (equation 3) stars. With this further selection our sample is composed of 60 539 disc stars.

Finally, we remind the reader that the photometric selection criteria of the APOGEE targets and the $T_{\rm eff}$-log g boundaries of the APOGEE Stellar Parameter and Chemical Abundances Pipeline grid may bias the resulting metallicity distribution, e.g. by undersampling the metal-rich tail at [M/H] $> +0.1$ dex, as discussed by Hayden et al. (2014). The radial metallicity gradients and the velocity–metallicity correlations, especially for the thin disc, could be sensitive to this effect and in particular at larger distances. We briefly address this issue in the next section.

[1]We adopt the overall chemical abundance [M/H] and α-element abundances [α/M], as derived by the APOGEE Stellar Parameter and Chemical Abundances Pipeline (ASPCAP, Zamora et al. 2015). The stellar parameters fitted by ASPCAP are $T_{\rm eff}$, log g, ξ_t, [M/H], [α/M], [C/M], and [N/M]. Here, the overall metallicity is defined as $[\mathrm{M/H}] = \log(\mathrm{N_M/N_H})_\star - \log(\mathrm{N_M/N_H})_\odot$, where N_M and N_H are the number density of all elements with atom number $Z > 2$ and hydrogen nuclei, respectively. The α-elements considered are O, Ne, Mg, Si, S, Ca, and Ti.

Downloaded from https://academic.oup.com/mnrasl/article/484/1/L69/5142291 by guest on 30 November 2020

Table 1. Radial metallicity gradients, ∂[M/H]/∂R in dex kpc^{-1}, in bins of R and $|z|$, for disc stars below $|z| = 3$ kpc.

Sample	$\|z\|$ kpc	R = 6 kpc		R = 8 kpc		R = 10 kpc		R = 12 kpc	
		N	∂[M/H]/∂R	N	∂[M/H]/∂R	N	∂[M/H]/∂R	N	∂[M/H]/∂R
Thin disc	≥1	99	−0.113 ± 0.044	1688	−0.031 ± 0.010	1557	−0.047 ± 0.009	1078	−0.010 ± 0.010
	<1	1291	−0.061 ± 0.009	19585	−0.013 ± 0.003	13985	−0.060 ± 0.003	5690	−0.039 ± 0.004
	all	1390	−0.073 ± 0.010	21273	−0.007 ± 0.003	15542	−0.062 ± 0.003	6768	−0.037 ± 0.004
Thick disc	≥1	1048	+0.021 ± 0.014	4612	+0.005 ± 0.007	1113	+0.022 ± 0.012	284	+0.031 ± 0.023
	<1	863	−0.017 ± 0.015	4270	0.000 ± 0.008	1438	−0.031 ± 0.011	281	0.000 ± 0.030
	all	1911	−0.023 ± 0.010	8882	+0.019 ± 0.005	2551	−0.012 ± 0.009	565	+0.011 ± 0.019

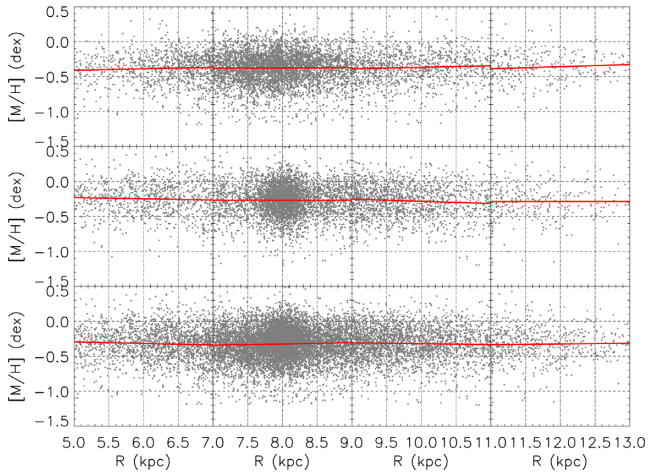

Figure 4. As Fig. 3, but for thick disc stars.

3 RESULTS

We focus on the sample within the Galactocentric (cylindrical) distance range $5 < R < 13$ kpc for a total of 58 882 disc stars. Also, the following analysis refers to four Galactocentric rings, each 2 kpc wide, with central radius at $R = 6, 8, 10, 12$ kpc, respectively. In addition, both chemically selected thin and thick disc stars are considered in three height intervals: $|z| < 3$ kpc, $|z| < 1$ kpc, and $1 \leq |z| < 3$ kpc.

Figs 3–4 show the distribution of [M/H] as a function of R, and the three z intervals above, for thin and thick disc stars, respectively. A linear fit to the data is also shown for each of the Galactocentric rings examined, while the actual fit results are provided in Table 1. At a given range, radial gradients appear consistent with trends expected for the two disc populations irrespective of distance from the Galactic plane. In particular, thick disc stars show rather flat (or mildly positive) gradients throughout the portion of the disc proved. Within the Solar annulus, $7 < R < 9$ kpc, we measure for the low-α (thin disc) population a radial metallicity gradient of -0.031 ± 0.010 dex kpc^{-1} in the range $1 \leq |z| < 3$ kpc, and of -0.013 ± 0.003 dex kpc^{-1} within $|z| < 1$ kpc. For the high-α population, the fit estimations go from a flat slope of 0.000 ± 0.008 dex kpc^{-1} for $|z| < 1$ kpc to a positive slope of 0.019 ± 0.005 dex kpc^{-1} below $|z| = 3$ kpc. These gradients are consistent with recent measurements like in, e.g. Anders et al. (2014), Recio-Blanco et al. (2014), Li & Zhao (2017), and Peng et al. (2018).

Figs 5–6 show the distribution of rotational velocity V_ϕ with [M/H] for thin and thick disc stars, respectively. The slope, $\partial V_\phi/\partial$[M/H], is estimated again via a linear fit to the data for each of the four MW rings and the three Galactic plane strips defined above. Table 2 provides the results of the fits and lists: total number of stars, slope (i.e. the velocity-metallicity gradients), and Spearman's rank correlation coefficient for each of the bin (in R and $|z|$) studied. We clearly notice *negative* velocity–metallicity correlations for thin disc stars at any $|z|$ and throughout the disc; the thick disc population shows quite a similar behaviour but for *positive* correlations. Moreover, as expected, V_ϕ slows down with increasing $|z|$ for both chemically selected populations.

At the Solar circle, i.e. $7 < R < 9$ kpc, a kinematics–metallicity correlation of 42.8 ± 3.4 km s^{-1} dex^{-1} is estimated for the thick disc in the range $1 \leq |z| < 3$ kpc, while a shallower slope 27.9 ± 3.2 km s^{-1} dex^{-1} is present within $|z| < 1$ kpc (see Fig. 6, second panels from the left). These estimates are quite compatible with the earlier measurements of Spagna et al. (2010), and later confirmed by a number of independent studies (Kordopatis et al. 2011; Lee et al. 2011; Adibekyan et al. 2013; Haywood et al. 2013; Kordopatis et al. 2013; Guiglion et al. 2015; Allende Prieto, Kawata & Cropper 2016; Wojno et al. 2016).

Finally, let us briefly address the issue of possible biases related to the known undersampling of the metal-rich tail of the APOGEE Survey (see end of Section 2). We tested the robustness of the findings above by repeating all of our linear least-squares fits after applying metallicity cuts [M/H] < [M/H]$_{\rm max}$, with 0.0 dex ≤ [M/H]$_{\rm max}$ ≤ 0.5 dex, to thin and thick disc star samples alike. Within the errors, all the fits appear quite consistent with the results we present in Tables 1 and 2; in other words, we do not find any statistically significant (propagated) bias affecting either the radial metallicity gradients or the rotation–metallicity correlations of both the thin and thick discs.

4 DISCUSSION AND CONCLUSIONS

By combining astrometric information from *Gaia* DR2 with radial velocities and chemical abundances from APOGEE DR14, we measured the radial metallicity gradients and, for the first time, the rotation metallicity correlation of the MW disc populations as a function of R in a relatively wide radial range spanning from 5 to 13 kpc.

We adopted the usual chemical classification method of thin and thick disc stars based on two main evolutionary sequences in the [α/M] versus [M/H] diagram (Fig. 1). The fact that the chemo-kinematical properties of these two populations are consistent near the Galactic plane and above 1 kpc from it shows the power of the α-elements-based classification criterion.

Concerning the radial metallicity gradient, our analysis of the new data confirm the negative slope for the thin disc and the flat (or mildly positive) slope for the thick, as found in previous studies based mainly on spectro-photometric distances (e.g. Carrell, Chen & Zhao 2012; Anders et al. 2014; Recio-Blanco et al. 2014; Li & Zhao 2017).

Downloaded from https://academic.oup.com/mnrasl/article/484/1/L69/5142291 by guest on 30 November 2020

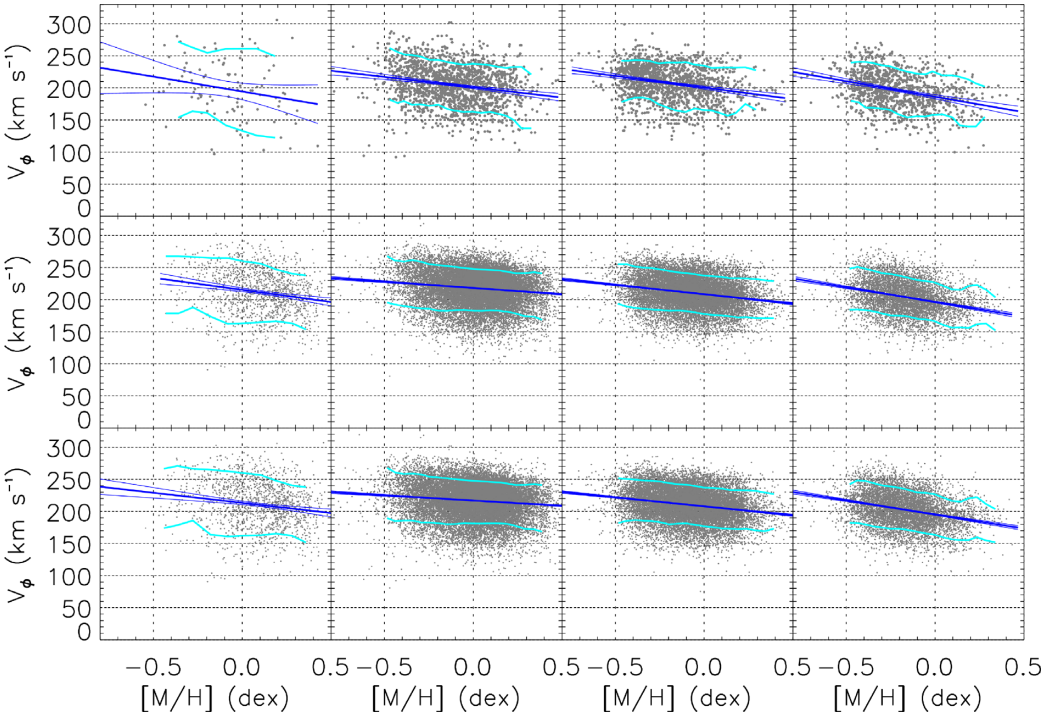

Figure 5. Velocity-metallicity distribution of thin disc stars as a function of Galactocentric (cylindrical) radius R, and distance from the plane $|z|$. The sample is shown, from left to right, in four 2 kpc wide rings at the central radii $R = 6$, 8, 10, 12 kpc. In the vertical direction, the bottom panels show stars with $|z| < 3$ kpc, the middle panels stars with $|z| < 1$ kpc, while the parts of the sample with $1 \leq |z| < 3$ kpc is given in the top panels. The solid blue lines represent the linear fits to the data and the corresponding 99 per cent confidence level curves. The solid cyan lines are the 10th and 90th percentiles of the data shown.

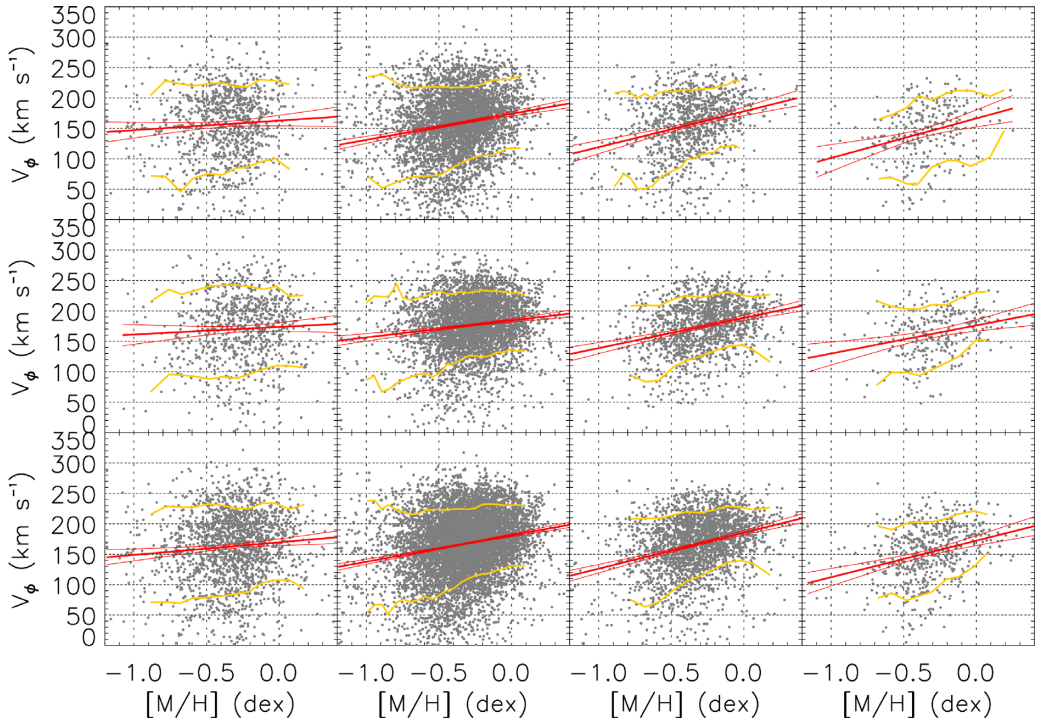

Figure 6. As Fig. 5, but for thick disc stars.

Downloaded from https://academic.oup.com/mnrasl/article/484/1/L69/5142291 by guest on 30 November 2020

Table 2. Rotation–metallicity correlations, $\partial V_\phi/\partial$[M/H] in km s^{-1} dex^{-1}, in bins of R and $|z|$, for disc stars below $|z| = 3$ kpc.

Sample	$\|z\|$ kpc	R = 6 kpc			R = 8 kpc			R = 10 kpc			R = 12 kpc		
		N	$\partial V_\phi/\partial$[M/H]	ρ_s	N	$\partial V_\phi/\partial$[M/H]	ρ_s	N	$\partial V_\phi/\partial$[M/H]	ρ_s	N	$\partial V_\phi/\partial$[M/H]	ρ_s
Thin	≥1	99	−46.4 ± 20.5	−0.22	1688	−32.2 ± 3.6	−0.23	1557	−36.1 ± 3.4	−0.27	1078	−48.4 ± 4.3	−0.33
	<1	1291	−37.7 ± 5.4	−0.20	19585	−19.5 ± 1.0	−0.13	13985	−29.3 ± 1.1	−0.22	5690	−45.8 ± 1.9	−0.30
	all	1390	−31.6 ± 5.1	−0.18	21273	−16.3 ± 1.0	−0.11	15542	−27.9 ± 1.0	−0.22	6768	−43.8 ± 1.8	−0.29
Thick	≥1	1048	+15.7 ± 7.6	+0.06	4612	+42.8 ± 3.4	+0.18	1113	+58.9 ± 6.3	+0.27	284	+65.1 ± 12.7	+0.33
	<1	863	+12.4 ± 7.9	+0.07	4270	+27.9 ± 3.2	+0.13	1438	+49.7 ± 4.7	+0.27	281	+46.2 ± 9.7	+0.29
	all	1911	+20.7 ± 5.3	+0.10	8882	+43.5 ± 2.3	+0.20	2551	+59.2 ± 3.7	+0.30	565	+60.1 ± 7.8	+0.34

As for the velocity–metallicity correlation, $\partial V_\phi/\partial$[M/H], that of the thin disc appears consistently *negative* throughout the radial range probed. This is in line with expectations given the negative sign of the corresponding chemical gradient exhibited in Fig. 3, and the radial oscillation of the individual stars caused by the epicyclic component due to blurring effects (e.g. Schoenrich & McMillan 2017; Kawata et al. 2018, and references therein).

The situation appears substantially different for the thick disc. To the best of our knowledge, Fig. 6 offers for the first time observational evidence that the circular velocity–metallicity correlation of the thick disc is persistently *positive* within the 8 kpc range of Galactocentric distances investigated, in spite of a quasi-flat metallicity gradient. This suggests that the chemo-kinematical mechanisms in place for the thin disc are probably replaced, totally or in part, by other processes (e.g. inside out formation) when dealing with the α-enhanced population as discussed by Schoenrich & McMillan (2017) and Kawata et al. (2018). Their simulations point out that the present-day radial metallicity and rotation–metallicity correlation of the ancient disc stars reflect the imprints of the cosmological conditions (i.e. the original metallicity gradient of the ISM and inside-out formation) convolved with the mechanisms of secular dynamical evolution of the MW disc, and with possible perturbations from satellite mergings.

To this regard, it is quite interesting to compare our Fig. 6 to fig. 8 in Kawata et al. (2018), whose first and third rows show a constant positive correlation versus R, which is associated with an almost flat present-day radial metallicity gradient, as per our Fig. 4. However, if we look at the two figures in greater detail, we notice that the observed thick disc rotation–metallicity correlation increases as a function of the galactic radius, while the simulations show an opposite trend.

Kawata et al. (2018) results derive from N-body MW-like simulations (their C1 and C2-thick1 models) that assume positive cosmological chemical gradients in the disc, as initially proposed by Curir et al. (2012). Finally, alternative scenarios, as those suggested by the analytical models of Schoenrich & McMillan (2017), also deserve further investigations possibly employing fully realistic cosmological simulations of the MW as in Murante et al. (2015).

There is no doubt that the results presented here will help setting crucial constraints on the origin and destiny of the Galactic disc in the context of cosmological models of MW formation.

ACKNOWLEDGEMENTS

We wish to thank the referee for a careful reading of this manuscript and for the useful comments that helped us improve on the original submission. This work has used data from the European Space Agency (ESA) mission Gaia (https://www.cosmos.esa.int/gaia), processed by the Gaia Data Processing and Analysis Consortium (DPAC, https://www.cosmos.esa.int/web/gaia/dpac/consortium). Funding for the DPAC has been provided by national institutions, in particular the institutions participating in the Gaia Multilateral Agreement. This work has been funded in part by the Italian Space Agency (ASI) under contract No. 2014-025-R.1.2015 'Gaia Mission – The Italian Participation to DPAC'. Funding for the Sloan Digital Sky Survey IV has been provided by the Alfred P. Sloan Foundation, the U.S. Department of Energy Office of Science, and the Participating Institutions. SDSS acknowledges support and resources from the Center for High-Performance Computing at the University of Utah. The SDSS web site is www.sdss.org. SDSS is managed by the Astrophysical Research Consortium for the Participating Institutions of the SDSS Collaboration including the Brazilian Participation Group, the Canergie Institution for Science, Canergie Mellon University, the Chilean Participation Group, the French Participation Group, Harvard-Smithsonian Center for Astrophysics, Instituto de Astrofísica de Canarias, The Johns Hopkins University, Kavli Insitute for the Physics and Mathematics of the Universe (IPMU) / University of Tokyo, the Korean Participation Group, Lawrence Berkeley National Laboratory, Leibniz Institut für Astrophysik Potsdam (AIP), Max-Plank-Institut für Astronomie (MPIA Heidelberg), Max-Plank-Institut füer Astrophysik (MPA Garching), Max-Plank-Institut für Extraterrestrische Physik (MPE), National Astronomical Observatories of China, New Mexico State University, New York University, University of Notre Dame, Observatório Nacional / MCTI, The Ohio State University, Pennsylvania State University, Shanghai Astronomical Observatory, United Kingdom Participation Group, Universidad Nacional Autonóma de México, University of Arizona, University of Colorado Boulder, University of Oxford, University of Portsmouth, University of Utah, University of Virginia, University of Washington, University of Wisconsin, Vanderbilt University, and Yale University.

REFERENCES

Abadi M. G., Navarro J. F., Steinmetz M., Eke V. R., 2003, ApJ, 597, 21
Abolfathi B. et al., 2018, ApJS, 235, 42
Adibekyan V. Z. et al., 2013, A&A, 554, A44
Allende Prieto C., Kawata D., Cropper M., 2016, A&A, 596, A98
Anders F. et al., 2014, A&A, 564, A115
Brook C. B., Gibson B. K., Martel H., Kawata D., 2005, ApJ, 630, 298
Carrell K., Chen Y., Zhao G., 2012, AJ, 144, 185
Curir A., Lattanzi M. L., Spagna A., Matteucci F., Murante G., Re Fiorentin P., Spitoni E., 2012, A&A, 545, A133
Gaia Collaboration, 2018, A&A, 616, A1
Garcia Perez A. E. et al., 2016, AJ, 151, 144
Gilmore G., Reid N., 1983, MNRAS, 202, 1025
Guiglion G. et al., 2015, A&A, 583, A91
Hayden M. R. et al., 2014, AJ, 147, 116
Haywood M., Di Matteo P., Lehnert M. D., Katz D., Gómez A., 2013, A&A, 560, A109
Haywood M., Di Matteo P., Snaith O., Lehnert M. D., 2015, A&A, 579, A5
Holtzman J. A. et al., 2015, AJ, 150, 148
Kawata D. et al., 2018, MNRAS, 473, 867
Kordopatis G. et al., 2011, A&A, 535, A107
Kordopatis G. et al., 2013, MNRAS, 436, 3231

Downloaded from https://academic.oup.com/mnrasl/article/484/1/L69/5142291 by guest on 30 November 2020

Kordopatis G., Wyse R. F. G., Chiappini C., Minchev I., Anders F., Santiago B., 2017, MNRAS, 467, 469
Lee Y. S. et al., 2011, ApJ, 738, 187
Li C., Zhao G., 2017, ApJ, 850, 25
Lindegren L. et al., 2018, A&A, 616, A2
Majewski S. R. et al., 2017, AJ, 154, 94
McMillan P. J., 2010, MNRAS, 465, 76
Minchev I., Steinmetz M., Chiappini C., Martig M., Anders F., Matijevic G., de Jong R. S., 2017, ApJ, 834, 27
Murante G., Monaco P., Borgani S., Tornatore L., Dolag K., Goz D., 2015, MNRAS, 447, 178
Peng X., Wu Z., Qi Z., Du C., Ma J., Zhou X., Jia Y., Wang S., 2018, PASP, 130, 74102
Recio-Blanco A. et al., 2014, A&A, 567, A5
Roskar R., Debattista V. P., Stinson G. S., Quinn T. R., Kaufmann T., Wadsley J., 2008, ApJ, 675, L65
Schoenrich R., Binney J., 2009, MNRAS, 396, 203
Schoenrich R., McMillan P. J., 2017, MNRAS, 467, 1154
Schoenrich R., Binney J., Dehnen W., 2010, MNRAS, 403, 1829
Spagna A., Lattanzi M. G., Re Fiorentin P., Smart R. L., 2010, A&A, 510, L4
Villalobos A., Helmi A., 2008, MNRAS, 391, 1806
Wojno J. et al., 2016, MNRAS, 461, 4246
Zamora O. et al., 2015, AJ, 149, 181
Zasowski G. et al., 2013, AJ, 146, 81

This paper has been typeset from a TEX/LATEX file prepared by the author.

Downloaded from https://academic.oup.com/mnrasl/article/484/1/L69/5142291 by guest on 30 November 2020